CERN/TCC/71-14
2 April 1971

NEUTRAL PION SPECTROSCOPY WITH BUBBLE CHAMBERS

H. Wenninger and H. Leutz
CERN, Geneva

Abstract

Several possibilities for neutral pion spectroscopy with bubble chambers were studied: electronic counters, conversion plates, and track sensitive targets. At present, the most promising facility with respect to gamma conversion probability and π^o- resolution efficiency was found to be a large cryogenic chamber filled with neon-hydrogen as conversion liquid and equipped with a track sensitive hydrogen target for the primary interactions. FAKE studies based on kinematical data of the 16 GeV (π^-p) - exposure at CERN indicate for BEBC an optimum target shape of the following dimensions: 3 m in beam direction, 1 m for beam spread and between 0.1 m and 0.15 m in the optics direction. In case of the 16 GeV (π^-p) - four prongs the 4C-fit efficiency increases from 14.5 $^o/o$ obtained in BEBC filled with hydrogen to 50 $^o/o$ with a 50 molar $^o/o$ neon-hydrogen mixture and a hydrogen target of optimum shape.

I. Introduction

At first sight, the data compilations now available for several elementary particle reactions, impress us by the striking pile up of symbols and digits. In spite of the enthusiasm induced by the expectations of still larger accelerators and still faster data acquisition we should, however, lower our sights and realize, that elementary particle spectroscopy rests at a level comparable with that of nuclear physics some 25 years ago. At that time the lack of efficient gamma detection prevented nuclear physicists from disentangling complex nuclear decay modes. Today, elementary particle detectors are strongly biased to charged particle identification and mostly miss the information associated with the neutrals. Consequently, deep inelastic collisions, which dominate at high energies and should, therefore, highly merit our attention, cannot be reasonably analysed due to the lack of neutral pion identification. The same is true for proton - antiproton annihilation, where about two thirds of the events involve two or more neutral pions as well as for the decays of strange particles, meson - and baryon resonances, where, in most cases, gammas and neutral pions are among the final state constituents.

Bubble chambers, in particular with hydrogen or deuterium fillings, prove to be highly resolving instruments for charged particles. They provide free protons and quasi free neutrons with full sensitivity in the target volume, subtend the total solid angle with almost isotropic detection efficiency, and offer high spatial and momentum resolution. They suffer, however, from the lack of neutral pion detection on account of the poor gamma conversion efficiency of hydrogen or deuterium. Heavy liquid chambers, in spite of yielding considerably higher conversion efficiency, cannot counterbalance this drawback because they are unable to serve our needs for simple target nuclei and high resolution.

With this in mind, we investigate in the course of this report, the possibilities for neutral pion spectroscopy with bubble chambers.

To demonstrate the claimed importance of this subject we start with neutral pion production in elementary particle reactions. Then, the basic difficulties of neutral pion spectroscopy are illustrated by treating the neutral pion decay mode in connection with higher π^o-multiplicities. Evidently, gamma spectroscopy dominates neutral pion identification and we therefore study gamma conversion and in particular the unambiguous association of gamma decay pairs. So as not to remain within a purely academic pattern we optimise appropriate detector arrangements by employing FAKE simulations based on experimental reaction kinematics. Finally, we try to integrate the explored method of neutral pion identification into the frame of elementary particle spectroscopy.

II. Neutral Pion Production

The fraction of events which contain neutral pions in their production channels increases with c.m.-energy. This becomes evident from fig. 1 which displays the fractions of $(\pi^{\pm} p)$ - total cross sections going into π^o- channels. The fractions of "no fits" due to the coincident production of more than one neutral particle are plotted in the same figure. At higher energies the "no fits" approach the curve representing the π^o- channels, thus proving that neutral pions mostly cause the unfitting events. About 65 °/o (90 °/o) unfitting events at 20 GeV/c (200 GeV/c) incident $\pi^{\pm}$ - momentum confront us with the problem of neutral pion spectroscopy. By missing the information contained in these π^o- channels the physics output of deep inelastic collisions becomes fairly poor.

Also, the number of coincidentally produced neutral pions increases with c.m.-energy. This is obvious from fig. 2 which contains the charged multiplicities computed by O. Czyzewsky and K. Rybicki[9] and the multiplicities of neutral pions calculated from π^o- cross sections σ_{π^o} which are quoted in the relevant papers[1-8]. In the neutron

channels we disentangled the single neutral pions from the multiply produced ones by correspondingly applying the cross-section ratios obtained from the proton channels in question. To account for the coincident production of more than two neutral pions we separated the appropriate production channels according to the predictions of the Poisson distributions. This procedure caused a slight correction only for beam momenta higher than 8 GeV/c. The curve fitted to the neutral pion multiplicities obtained in this way yiels the c.m.-energy dependence

$$\langle n_{\pi^0} \rangle = \frac{\sum n_{\pi^0} \sigma_{\pi^0}}{\sum \sigma_{\pi^0}} = E^{0.35}$$

which allows extrapolation to higher c.m.-energies. In the region of CERN-PS beam momenta the π^0-multiplicity is almost two. At the CERN-PS we should therefore mainly be concerned with the spectroscopy of two coincidentally produced neutral pions. For beam momenta between 100 GeV/c and 400 GeV/c, shortly available at Batavia, the π^0-multiplicity centers around three and the charged multiplicity around ten. This opens exciting prospects for the computer industry.

Finally, the neutral pion momentum distribution reflects on the design criteria of an appropriate detector. Due to the lack of π^0- identification the information on this subject is restricted to 1C-fit results of single π^0- production. The π^0- momenta from 4 prong channels of the 8 GeV/c[6] and 16 GeV/c[7] $(\pi^+ p)$- reactions are plotted in fig. 3 as fractions of the relevant beam momenta. Both distributions are normalized to the same total of events. From these distributions it becomes evident that the π^0- momenta do not simply increase with the beam momentum. A 40 °/o fraction of low momentum neutral pions exhibits even a rather constant distribution. From the momentum distributions of charged pions we assume that this behaviour will be even more pronounced for multiple π^0- production. The frequency of low momentum neutral pions expected for even higher beam momenta results in noticeable transverse momenta and rather large opening angles between the gamma decay pair. This asks for π^0- detection subtending the entire solid angle.

III. Neutral Pion Decay

The neutral pion, being at the same time its own anti particle, decays after a mean lifetime of $(0.76 \pm 0.15) \times 10^{-16}$ sec with a rate of (98.83 ± 0.04) °/o into two gamma quanta. Even with 100 GeV/c momentum it would traverse only 17μm in real space and hence within the spatial resolution of bubble chambers the π^o- production co-ordinates can be considered identical with the decay co-ordinates. The decay modes into $\gamma + e^- + e^+$ (1.17 °/o); 2 $(e^- + e^+)$; or 3 γ can be disregarded in the context of these considerations. In the c.m. system the two gammas are emitted in opposite directions which are, due to the zero spin of the neutral pion, isotropically distributed:

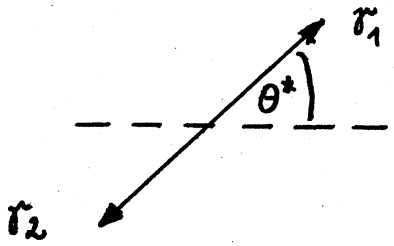

Transformation into the Lab-system yields from the π^o- momentum $P_{\pi o}$ the respective gamma momenta Σ_1 and Σ_2, from the c.m. - decay angle θ^* the opening angle θ, and the angle ξ between the π^o- direction and the straight line bisecting the gamma opening angle:

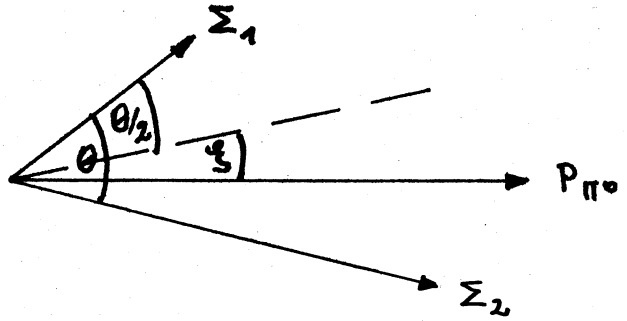

by employing energy - and momentum conservation we obtain:

$$\Sigma_1 \Sigma_2 (1 - \cos\theta) = \frac{m_{\pi o}^2}{2} \qquad (1)$$

with m_{π^o} meaning the π^o- rest mass. Expanding to n neutral pions and hence 2n gammas emerging from the same decay point leads to:

$$\sum_{\substack{i,k=1 \\ i<k}}^{2n} \Sigma_i \Sigma_k X_{i,k} = m_{\pi^o}^2 \left[\frac{n}{2} + \sum_{\substack{\mu,\nu=1 \\ \mu<\nu}}^{n} \gamma_\mu \gamma_\nu \left(1 - \beta_\mu \beta_\nu \cos \vartheta_{\mu,\nu}\right) \right] \qquad (2)$$

where $X_{i,k} = 1 - \cos \theta_{i,k}$, and $\theta_{i,k}$ means the angle between the i - th and k - th gamma. $\vartheta_{\mu,\nu}$ has the corresponding meaning for the angle between two neutral pions. $\beta_{\mu,\nu}$ indicates the relativistic π^o- velocity and $\gamma_{\mu,\nu}$ the total π^o- mass in units of the π^o- rest mass.

Relation (1), which holds for a single π^o- decay, represents a clear connection between the opening angle and the two gamma momenta. With the two gamma directions and with one gamma energy we are able to evaluate the π^o- momentum. By looking at the coincident decays of n neutral pions (relation 2) we realize that knowledge of more parameters is necessary to disentangle the n (2n - 1) possible pairing combinations *). Therefore we need to associate the gammas to decay pairs by applying the following χ^2 fit[10]:

$$\chi^2 = \frac{\left(\Sigma(m)_1 - \Sigma(\xi)_1\right)^2}{2\left(\Delta\Sigma(m)_1\right)^2} + \frac{\left(\Sigma(m)_2 - \Sigma(\xi)_2\right)^2}{2\left(\Delta\Sigma(m)_2\right)^2} \qquad (3)$$

with $\Sigma(m)_{1,2}$ meaning the gamma momenta measured with the error $\Delta\Sigma(m)_{1,2}$ via the (e^-, e^+) - conversion pair and the corresponding gamma momenta $\Sigma(\xi)_{1,2}$ resulting from the π^o- and gamma directions:

$$\Sigma(\xi)_{1,2} = \frac{m_{\pi^o}}{2 \sin \theta/2} \left(\frac{\sin\left(\theta/2 \pm \xi/3\right)}{\sin\left(\theta/2 \mp \xi/3\right)} \right)^{1/2} \qquad (3a)$$

*) Conversion of one gamma out of four (from two neutral pions) does not provide any additional information. This is obvious from relations (2) and (3). This is still true for a statistically meaningful sample of such events because knowledge of one gamma momentum does not improve the event fit efficiency for the $2\pi^o$- channel as shown in reference (22).

With the fit procedure of relation (3), which necessitates the measurement of all gamma momenta involved, we optimize at a fixed angle θ the gamma momenta by evaluating χ^2 (ξ opt) = χ^2 Min (ξ). To associate the gamma decay pairs with the parent - π^o we fit all the possible n(2n- 1) angles θ_i. The angle θ_{opt} yielding the smallest χ^2 is then the most probable gamma association and this probability corresponds to the pairing efficiency achievable with the detector in question (see fig. 11). After the filtre provided by the χ^2- fit, relation (2) can be reduced into the much simpler arrangement for n known gamma pairs:

$$\sum_{i=1}^{n} \Sigma_{(2i-1)} \Sigma_{2i} \chi_{(2i-1),2i} = \frac{n}{2} m^2_{\pi^o} \qquad (4)$$

Relation (4) immediately follows from relation (2) if we assume Σ_i and Σ_k to be a decay pair which belongs to π^o ($\gamma_\mu = 0$).

According to relations (2) and (4) we need 2n converted gammas from n produced neutral pions and, according to relation (3b), the knowledge of 2n gamma momenta and 2n gamma directions to unambiguously associate the gamma decay pairs and to finally evaluate the n π^o- momenta. Together with the data determined from the tracks of the charged particles we then obtain what is in general called a four constraint* (4C) fit of the bubble chamber event in question.

Now, the conversion of all 2n gammas requires a comparatively high conversion probability

$$P^{2n}_{2n} = q^{2n} \qquad (5)$$

---

* The additional two constraints emerging from the knowledge of all gamma directions and energies have been used to associate the gamma pairs with their parent neutral pions.

with $q = 1 - e^{-\pi d}$ meaning the pair conversion probability for a single gamma, if π stands for the pair conversion coefficient and d for the thickness of the available conversion layer.

The conversion probability for 2n - 1 gammas out of 2n gammas amounts to:

$$P^{2n}_{2n-1} = 2n\, q^{2n-1} (1-q) \qquad (5a)$$

and for the two cases in question we obtain the probability ratio:

$$P^{2n}_{2n-1} \Big/ P^{2n}_{2n} = 2n \frac{1-q}{q}$$

which, by setting $e^{-\pi d} = e^{-7/9 \frac{L}{X_0}}$ (which is true only for infinitely high gamma energies) simplifies to:

$$P^{2n}_{2n-1} \Big/ P^{2n}_{2n} = \frac{2n}{e^{7/9\, L/X_0} - 1} \qquad (5b)$$

Relation (5b) shows, that in case of n = 2 π^0 and $\frac{L}{X_0} = 1.4$ (which corresponds approximately to 30 molar $^0/_0$ neon fraction in BEBC) the conversion probability for 2n-1 gammas out of 2n gammas is about 2 times higher than the conversion probability for 2n gammas. Of course, for $\frac{L}{X_0} = 2.4$ (corresponding to a 50 molar $^0/_0$ neon fraction in BEBC) the ratio reduces to 0.8.

Therefore, one gamma out of 2n will escape more or less frequently depending on the conversion layer available in the neutral pion detector, and we shall miss the associated neutral pion. The

event fit is then reduced to one constraint (1C)*), which is still sufficient to completely determine all event parameters but does not allow cross-checks to refuse ambiguous constellations, i.e. the value of 1C-fits depends very much on the details of the particular event. Again, we employ the χ^2-fit of relations (3) and (3a) to disentangle the n (2n -2) +1 gamma combinations which could form a decay pair out of the 2n-1 converted gammas.

Apart from the above described gamma association, which demonstrates the importance of gamma momentum measurements, the opening angle θ is also relevant for the design of a π^o- detector. By appropriate treatment of π^o- decay kinematics we obtain:

$$\sin \frac{\theta}{2} = \frac{1}{\gamma \sqrt{1 - \beta^2 S^2}} \qquad (6)$$

with S meaning the probability for gamma emission into the angular interval between θ and the minimum opening angle θ min, which, in the c.m.-system, corresponds to gamma emission transverse to the π^o- direction ($\sin \frac{\theta \text{ min}}{2} = \frac{1}{\gamma}$). The probability S is linked to the c.m. decay angle θ^* via $S = \cos \theta^*$ and therefore in turn describes how the π^o- momentum is shared between the two gammas: $S = \frac{1}{P\pi^o} (\Sigma_1 - \Sigma_2)$. A relation similar to relation (6) holds for the angle ξ between the π^o- direction and the direction bisecting the opening angle θ:

$$\sin \xi = \frac{S}{\gamma \sqrt{1 - \beta^2 S^2}} = S \sin \theta/2$$

Fig. 4 displays the probabilities for the gamma opening angles in dependence from the π^o- momentum and illustrates that a considerable fraction of gammas is emitted with rather large transverse momenta.

---

*) This is still true even for two escaping gammas if the converted 2 (n - 1) gammas belong to n-1 decay pairs. However, for efficient conversion layers, i.e. $L/X_o > 2$, this probability represents a small fraction only as compared to that of 2n-1 converted gammas: $(2\, e^{7/9\, L/X_o} - 1)^{-1}$.

Of course, we should also pay attention to the lab. angular gamma distribution with respect to the primary beam direction. Since this behaviour cannot be covered with one formula - the π^o- momenta come into the game-, we must consult experimental results. Fig. 5 compares the gamma angular distributions resulting from 1C-fits for the 4prong π^o- channels of the 8 and 16 GeV/c π^+p- reaction. Although the 16 GeV/c - distribution peaks at smaller angles than the 8 GeV/c one, we notice that still about 40 $^o/o$ of all gammas emerge with angles larger than 250 mrad. This corresponds at 1.5 m mean conversion path to a deviation of about 40 cm transverse to beam direction. This behaviour would be of course even more pronounced if we could have used the yet unknown channels containing the coincident production of two or three neutral pions. Moreover, those neutral pions emerging from high-mass resonant states can be emitted at large angles to the beamdirection. As a result, the neutral pion detector should be able to subtend the whole solid angle otherwise a large fraction of interesting events will remain undetected.

IV. Pattern Simulation with FAKE

From π^o- production and π^o- decay we realize that certain questions associated with these problems cannot be treated adequately by taking into account the isolated event only. Since all these processes are basically dominated by statistics we must process a statistically meaningful sample of events in order to obtain a clear picture of the necessary π^o- detection facility. Therefore, we used FAKE in connection with the kinematics data accessible from the 16 GeV/c (π^-p) - Data Summary Tape (DST). We transferred the events photographed in the CERN 2m - hydrogen chamber into the space of other detectors - mainly the Big European Bubble Chamber (BEBC) - by applying the following manipulations:

Vertex positions, production angles, particle trajectories, and secondary masses were projected into the new detector by maintaining corresponding proportions for the space coordinates and the true values

for the angles. The entries for the external error matrices were changed corresponding to the requirements of the detector in question; e.g. in case of BEBC the magnetic flux density was enlarged from 1.8T (2m- chamber) to 3.5T and the setting error was increased from 50μm (2m- chamber) to 300 μm. If stopping tracks permitted range measurements, those were preferred to curvature determination. Secondary track lengths were limited by taking into account 40 mb cross-section.

Since the 16 GeV - DST did not provide us with π^o- kinematics we had to simulate these data in the following way: In the six prong channels two pions of opposite charge were regarded as being neutral pions. Then, with a Monte Carlo generator, random gamma decay angles were produced in the c.m.-system. Those were transferred into the lab. system and the corresponding gamma momenta were computed. The conversion probability for each generated gamma quantum was calculated within the detector's boundary conditions. This was performed by applying the energy dependent pair production coefficient rather than the total gamma attenuation coefficient or the gamma conversion length 7/9 X_o (X_o = rad. length of the traversed material) which holds only at the limit of infinite gamma momentum.

The electron-positron conversion pairs were simulated by splitting the gamma momenta according to the well known electron momentum probability distribution. Finally, the electron momentum errors were computed by evaluating the optimum track length and by applying the Y_o- cut as proposed by Morellet[11] for the radiation loss.

The missing mass resolutions indicated in figs 8, 10 and 13, were obtained by presupposing the squared missing mass distributions of the fitted events to have Gaussian shape. Then the square root of the full width at half maximum (FWHM) of these distributions, which included about 2000 events for each configuration, was computed and represents the missing mass indicated in the above mentioned figures. Care has been taken to keep the fraction of background events, which had to be discarded, at a rather constant level of about 15 % for all plots.

V. Gamma Detection

Information on neutral pions can be gained only via the emerging decay gammas. The merits of a π^o- detector must therefore be classified with respect to its gamma conversion efficiency and to its gamma momentum resolution. In basing the design of our particle spectrometer on a bubble chamber as a sensitive beam target with high resolving power for charged secondaries we are left, for π^o- identification, with two possibilities: To convert and measure the decay gammas inside or outside the sensitive bubble chamber volume.

V.1. Gamma Detection outside the Bubble Chamber

The intention is to display the primary interaction within the sensitive volume and to measure the decay gammas in electronic detectors surrounding the bubble chamber. Before entering these electronic devices the gammas must traverse the chamber body wall and hence, gamma transmission probability plays an important role. Since we have to cope with an average π^o- multiplicity of two at the CERN Proton Synchrotron and of three at future accelerators we must take into account the transmission probabilities for four and six decay gammas, which are displayed in fig. 6. A wall thickness corresponding to more than 0.3 radiation lengths (in case of 3 π^o) or 0.5 radiation lengths (in case of 2 π^o) reduces the gamma transmission to less than 25 $^o/_o$. This means that the total wall thickness of chamber body and vacuum tank should not exceed 6 mm or 10 mm of steel.

Employing the chamber body wall as conversion plate does not really improve the situation. The uncertainty in locating the gamma conversion point within the wall does not permit even the above mentioned thickness. Moreover, the conversion pairs should then be detected close to the chamber wall which becomes complicated because of the requirements for chamber optics, thermal insulation and the magnetic field. These restrictions are true for all existing bubble chambers and

it is fair to state that they are useless for outside π^0- detection as well as for most other combinations with external counters running under the slogan of hybrid detectors. Only bubble chambers designed in particular for sufficient particle and gamma transmission over almost the total solid angle would be suited to match the requirements of external detection efficiency.

V.2. Gamma Detection inside the Bubble Chamber

In terms of gamma conversion efficiency the heavy liquid chamber is distinctly superior to the hydrogen/deuterium chamber. If we, however, aim at conserving the fundamental advantages - simple target nuclei, high resolution - of hydrogen/deuterium chambers we are, at the time being, left with three solutions:

- electronic counters in liquid hydrogen/deuterium
- plate arrangements in liquid hydrogen/deuterium
- track sensitive hydrogen/deuterium targets surrounded by hydrogen-neon mixtures.

By the first alternative we mean gamma momentum measurement with electronic counters immersed in the chamber liquid. The gamma conversion could then occur either directly in these detectors or in conversion plates mounted in front of them. When carefully reviewing counter types currently available we must discard all facilities based on light detection with photomultipliers, because these are not operative within the chamber magnetic field, and also on electron multiplication or spark ignition in gas fillings, which would liquify or solidify on cooling down to $25^{\circ}K$. Appropriate thermal insulations to overcome the last mentioned difficulty would result in space consuming vacuum chambers or plastic layers which would destroy the necessary spatial and momentum resolution of the counters. Finally, we are left with the range of solid state detectors which consists of silicon surface barrier diodes and

lithium drifted germanium crystals. Total absorption of the cascade shower following the gamma conversion asks for about 10 radiation lengths sensitive depth which corresponds to 85 cm silicon or 23 cm germanium. Such detector layers are not at all feasible. Therefore, as an alternative solution, we could arrange the solid state counters as ionization - sensitive conversion plates in the chamber, which register the energy deposited by the conversion pair in the conversion layer and allow photographing of electron-positron pairs when they enter the hydrogen.

Plate arrangements have been widely discussed in other papers [10, 12, 13] and some of the experience with plate exposures in bubble chambers gained up to now has been recently summarized by D. Miller[14]. Their basic drawbacks are due to their geometrical arrangement, which is dictated by the requirements of beam trajectories, chamber optics, hydrodynamics, and chamber shape. This imposes restrictions upon the number, separation and adjustment of the plates and of the subtended solid angle. In turn, this reflects on the gamma detection efficiency and on the gamma momentum resolution which are considerably worse with plate arrays (see: Gamma momentum errors) as compared to a track sensitive conversion liquid with its density matched to the chamber geometrical dimensions.

A track sensitive conversion liquid becomes a practical possibility in the design of a composite chamber[15], where the interaction region consists of liquid hydrogen or deuterium and the surrounding neon-hydrogen mixture provides the gamma conversion layer. Such a device has been proposed in 1966[16] and its design features were based on the following requirements: To keep the composite chamber in the range of reliable operation conditions the track sensitive target has to be integrated as a passive element into the bubble chamber. The walls of the target container must be transparent to visible light to allow photographing tracks in both liquids with one common optical system and they should not cause an appreciable number of particle interactions.

To obviate temperature differences between target - and conversion liquid and to avoid a separate expansion system accurately synchronized with that of the chamber both liquids should become sensitive for track formation under identical operating conditions.

Two kinds of track sensitive targets have been operated in the meantime with their design criteria based on the above mentioned features: Flat rectangular shaped ones which transmit the expansion cycle through flexible walls*); cylindrical and rigid ones, which provide pressure transmission via attached metal bellows. Besides the basic differences in pressure transmission, shape, and wall thickness the two types also differ with respect to the covered neon-hydrogen mixture ratios: since the flexible targets do not allow for pressure differences between target and conversion liquid their operation parameters coincide for neon fractions which correspond to radiation lengths between 10 m and 45 cm. By running the hydrogen target 1°K colder than the mixture, which should be feasible with a heat exchanger inside the target bag, the flat targets could probably be immersed in a conversion liquid with 85 molar °/o neon content (33 cm radiation length). The cylindrical targets probably tolerate pressure differences which possibly enable operation with practically pure neon (28 cm radiation length) as conversion liquid.

The geometrical dimensions of track sensitive targets must be balanced so as to meet at the same time the demands for the fiducial volume to be provided for beam trajectories and primary interactions, for momentum resolutions of charged secondaries (which should not be considerably worse than those obtained with an entire hydrogen filling), and for the conversion paths of the emerging gammas, which should enter as early as possible into the dense mixture. For this optimization the flat rectangular bags provide three and the rigid cylinders two geometrical dimensions.

---

*) The expansion ratio $\Delta V/V$ for hydrogen/deuterium chambers amounts to 0.5 - 0.7 °/o. Consequently, the average Z-displacement of one target wall ranges between 250 µm and 350 µm at 10 cm target depth.

The bag dimension perpendicular to the beam and to the magnetic field direction, which corresponds to the cylinder diameter, is determined by the needs for beam sagitta and beam spread. To facilitate the back pointing of conversion pairs and hence to improve the discrimination against gamma background, mostly arising from bremsstrahlung quanta, the beam should have the largest possible spread. In large chambers like BEBC, we should ask for at least 70 cm beam spread which adds up together with some 15 cm beam sagitta and some clearance from the target wall to about 100 cm.

The dimension along the beam direction concerns the fraction of neon background events (which depends on the ratio of the corresponding cross-sections and of beam lengths in target and mixture), and the precision in curvature measurements of the fast secondaries, which strongly affect the missing mass resolution. Both aspects ask for the largest possible target length which must be balanced against the opposing need for sufficient gamma conversion behind the target. Figs. 7 and 8 show the corresponding FAKE results on conversion efficiency and on missing mass-resolution in dependence from the target length. They indicate an optimum target length of about 300 cm for BEBC filled with mixtures ranging from 30 molar $^{o}/_{o}$ (120 cm rad. length) to 70 molar $^{o}/_{o}$ (45 cm rad. length) neon, which keeps the fraction of neon background events well below 50 $^{o}/_{o}$.

The rectangular targets offer in addition a third geometrical dimension for shape optimization: the height of the bag transverse to the beam but aligned with the magnetic field and optics. This direction yields only poor spatial resolution and no magnetic bending power at all. Therefore, we must not ask for any beam spread or track length for curvature measurements in this direction. The target height reflects, however, on the angular precision of charged secondaries and it dominates in the opposite sense the gamma conversion path length and the stopping power available for range measurement candidates in the mixture. By again consulting the corresponding FAKE results displayed in figs 9

and 10 we learn that the optimum target height ranges between 10 cm and 15 cm in BEBC filled with 30 to 70 molar $^{o}/_{o}$ neon. To determine the production angles of the charged secondaries we employed the conventional procedure, which eliminates the influence of the magnetic field on the particle direction by momentum measurement via track curvature. Because of the multiple scattering the curvature measurements are restricted to the hydrogen volume only and therefore the target height reflects mainly on the angular precision. This situation could be improved considerably if we would correct for the magnetic deflection with particle momenta obtained via range measurements in the neon-hydrogen mixture. This could result in target heights between 5 and 10 cm yielding the same missing mass resolution than the above mentioned dimensions, but increasing the gamma conversion efficiency.

From the same figures we notice that dimensions of about 100 cm drastically reduce the gamma conversion efficiency without reasonably improving in missing mass resolution. Consequently, cylindrical targets, which need about 100 cm in diameter due to the beam requirements, cannot be matched appropriately for the most efficient gamma detection. This draw-back cannot be counterbalanced by even reducing the radiation length of the conversion liquid down to 28 cm (fig. 9).

VI. Gamma Momentum Errors

The π^o- momentum error ΔP_{π^o} is closely connected with the gamma momentum error $\Delta\Sigma$ via:

$$\left(\frac{\Delta p}{p}\right)_{\pi^o} = \frac{S}{\sqrt{\left(\frac{\Sigma_1}{\Delta\Sigma_1}\right)^2 + \left(\frac{\Sigma_2}{\Delta\Sigma_2}\right)^2}} \qquad (6)$$

with S being the probability of gamma emission into the angular interval θ and θmin (see fig. 4), which describes how the original π^o- momentum is shared between the decay gammas: $S = \frac{1}{P_{\pi^o}}(\Sigma_1 - \Sigma_2) = \frac{\sin\xi}{\sin\theta/2}$. Relation (6) represents the minimized π^o- error because it includes via S already the angular correlations between gamma and π^o- directions.

As stated already, the gamma momentum error dominates the gamma pairing procedure, which in turn represents the key for disentangling the n (2n - 1) gamma combinations resulting from n coincidentally produced neutral pions. Fig. 11 shows the influence of the gamma error on the pairing efficiency. The gamma angular and momentum distributions were taken from FAKE based on the 16 GeV/c DST and were filtered through the earlier meantioned (relation (3)) χ^2-fit. By this procedure we did not account for errors on the gamma directions. This is permitted with the spatial resolution obtained in track sensitive conversion liquids; with conversion plates, the uncertainty in the conversion point causes, depending on plate thickness, noticeable errors on the gamma directions.

The gamma momenta can be determined via their electron-positron conversion pairs only, either by measuring the resulting track curvatures of the first converted pair or by evaluating the integral energy loss which subsequently created conversion pairs suffer from traversing a known material layer. The latter procedure, usually referred to as the total track length method[17, 18, 19], asks for a sufficient material layer to ensure the absorption of a significant energy fraction of the cascade shower,

which propagates via subsequent generations of conversion pairs. To obtain reliable relations between the initial gamma momentum and the summed energy loss, needs a material thickness which corresponds to at least 5 radiation lengths. This is just achievable in BEBC filled with pure neon and yields about 15 °/o to 20 °/o relative gamma momentum error[18] which results, according to fig. 11, in a rather poor pairing efficiency. We, therefore, prefer to rely on gamma momentum determination via track curvature measurements of the first converted pair which result in the following relative electron (positron) momentum error:

$$\left(\frac{\Delta p}{p}\right)_e^2 = \frac{3.6\, p_e^2\, \varepsilon^2}{B^2 L^4} + \frac{2.6 \cdot 10^3}{B^2 L X_0} + \frac{Y_0^2 L}{6 \ln 2 X_0} \qquad (7)$$

with P_e meaning the electron momentum in GeV/c, B the magnetic flux density in kG, L the measured track length in cm and ϵ the setting error in µm. The third term, which represents the error caused by radiation loss, is estimated by employing the Behr-Mittner Method. In this case, collision loss is omitted, L/X_o is being considered small as compared to one, and the Yo- cut off is taken at 0.3. Neglecting the second term of relation (7), which accounts for multiple scattering, and balancing the first term, which represents the measuring error in case of eight optimally spaced measuring points, with the radiation loss results in the optimum track length:

$$L_{opt} = 3.5 \left(\frac{p_e \varepsilon}{B}\right)^{2/5} X_0^{1/5} \qquad (8)$$

which in turn yields the minimum electron (positron) momentum error in a conversion liquid:

$$\left(\frac{\Delta p_e}{p_e}\right)^{min}_{Liquid} = 0.31 \left(\frac{p_e \varepsilon}{B}\right)^{1/5} X_0^{-2/5} \qquad (9)$$

If we transform the radiation length X_o of the conversion liquid into $D/_n$, where D means the depth of the conversion layer available in the chamber and n the number of radiation lengths contained in this layer, we obtain the minimum gamma momentum error in a conversion liquid:

$$\left(\frac{\Delta\Sigma}{\Sigma}\right)^{min}_{Liquid} = 0.22 \left(\frac{\Sigma\varepsilon}{2B}\right)^{1/5} \left(\frac{n}{D}\right)^{2/5} \qquad (9a)$$

In this case we assume that the gamma momentum is equally shared between the electron and the positron momentum. Of course, we should always keep in mind that we have obtained relations (8), (9) and (9a) by sacrificing the multiple scattering term and by applying the Behr-Mittner method with a Y_o-cut off at 0.3 to account for the radiation loss. By basing this curvature measurement procedure on 300 µm setting error and on 35 kG magnetic flux density we may expect relative gamma momentum errors which range between 12 °/o and 5 °/o at chamber fillings corresponding to radiation lengths between 30 cm and 120 cm.

By arranging plates within a chamber filled with hydrogen or deuterium we aim at converting the gammas within these plates and at measuring the curvature of the first converted electron-positron pair within the gap of two subsequent plates. This results in the relative gamma momentum error:

$$\left(\frac{\Delta\Sigma}{\Sigma}\right)^2_{Plates} = P^2 + \frac{1}{2}\left(\frac{\Delta P_e}{P_e}\right)^2 \qquad (10)$$

The first term of relation (10) refers to the gamma error due to the uncertainty in the gamma conversion point and due to radiation loss fluctuations of the electron and positron within the plate material. According to Trilling[10] this term yields:

$$P = 0.6\, t / X_0^P \qquad (11)$$

with t being the plate thickness and X_0^P the radiation length of the plate material. The second term in relation (10) represents the errors due to electron-positron curvature measurements in the gap between two subsequent plates, again assuming equal gamma momentum shares within the conversion pair.

According to G.Trilling[10] (see also C. Fisher[13]) the best situation occurs for minimal curvature errors and matched errors from the plates, if we ask for the optimum plate thickness t and plate separation d at a given detector volume containing n radiation lengths of conversion material with the radiation length X_0^P. With this in mind, one obtains with a hydrogen filling

$$\left(\frac{\Delta\Sigma}{\Sigma}\right)^{min}_{Plates} = 1.1 \left(\frac{\Sigma\varepsilon}{2B}\right)^{1/3} \left(\frac{t}{X_0^P d}\right)^{2/3} \qquad (12)$$

by omitting the contributions of multiple scattering and radiation loss to the curvature error, which is in a first approximation tolerable for liquid hydrogen. Introduction of the total depth $D = n\, X_0^P\, d/t$ (which we measure in cm) for the plate array yields:

$$\left(\frac{\Delta\Sigma}{\Sigma}\right)^{min}_{Plates} = 1.1 \left(\frac{n}{D}\right)^{2/3} \left(\frac{\Sigma\varepsilon}{2B}\right)^{1/3} \qquad (13)$$

In comparing this optimised arrangement (which requires $0.71 \left(2n\, B/\Sigma\varepsilon\right)^{1/3} D^{2/3}$ plates) with a continuously sensitive conversion liquid we obtain with relations (9a) and (13) for the ratio of gamma momentum errors:

$$\frac{(\Delta\Sigma)_{Plates}}{(\Delta\Sigma)_{Liquid}} = 5.1\left(\frac{\Sigma\varepsilon}{2B}\right)^{2/15}\left(\frac{n}{D}\right)^{4/15} \qquad (14)$$

Relation (14) presupposes identical conditions for gamma momentum, magnetic flux density, and setting error as well as equal geometrical dimensions and conversion efficencies for the detector.

In optimising the plate array we still have disregarded the implications imposed by beam trajectories, optics, hydro-dynamics, and chamber shape on a practical arrangement. These requirements reduce the number of plates from 15, as assumed in the above considered academic case with D = 150 cm and n = 2, down to five as proposed by Leutz and Rau[12] for BEBC. The resulting gamma momentum error is then dominated by the uncertainty in the gamma conversion point (relation (11) and amounts to about 25 °/o).

VII. Missing Mass Fits.

From a composite chamber filled with 50 molar °/o neon fraction of conversion mixture we expect 8 °/o average gamma momentum error. According to relation (6), this results in about 4 °/o relative π^o- momentum error if we take the case S = 0.5, which corresponds to the statistical average for the gamma directions.

However, such considerations represent a rather isolated view of the neutral pion problem. In order to obtain a more realistic picture we must integrate the expected neutral pion mass resolution into the entire event fits. At the present level of elementary particle spectroscopy this is not possible with experimental results and we are again obliged to rely for a first approach on FAKE studies. The basic question to be posed is: How does the probably obtained π^o- resolution reflect on the missing mass fit of the entire event ? Following the

standard procedure, which compares the total mass before (labeled 0) with that after (labeled S) the reaction we obtain the squared missing mass:

$$m^2 = (E_o - E_s)^2 - (\vec{P}_o - \vec{P}_s)^2$$

By splitting the total energy E_s and momentum $\vec{P}_s$ of the secondaries into $E_s^{\,1} + E_{\pi o}$ and $\vec{P}_s^{\,1} + \vec{P}_{\pi o}$ we introduce separatly π^o- energy $E_{\pi o}$, π^o- momentum $\vec{P}\pi^o$, and the corresponding symbols $E_s^{\,1}$ and $P_s^{\,1}$ for the charged secondaries, which results in:

$$m^2 = (E_o - E'_s - E_{\pi o})^2 - (P_o - P'_s - P_{\pi o})^2$$

if we omit for simplicity the corresponding transverse momenta which presupposes that the angles in question are small and their cosines do not sensibly differ from one.

With Y and Z meaning the neutral pions energy and momentum fraction, resp., we obtain:

$$m^2 = \left[(1-Y)\,\Delta'_s + Y\,\Delta_{\pi o}\right]^2 - \left[(1-Z)\,\sigma'_s + Z\,\sigma_{\pi o}\right]^2$$

if we associate the errors Δ and σ with energies and momenta, resp. Taking the neutral pion errors X times those assumed for the other secondaries yields:

$$m^2 = (\Delta'_s)^2\,(1-Y+XY)^2 - (\sigma'_s)^2\,(1-Z+XZ)^2$$

which, finally, if we assume equal energy and momentum fractions (Z = Y), results in:

$$m = (1 - y + xy)\left((\Delta_s')^2 - (\sigma_s')^2\right)^{1/2} \qquad (15)$$

Relation (15) tells us in a first approximation the average impact of the neutral pion errors on the missing mass.

Of course, we must always bear in mind that relation (15) was deduced from simplified assumptions and therefore reflects the dependence of the missing mass from the neutral pion error in a rather qualitative manner only. To obtain for BEBC a result which is not disturbed by the above applied treatment we runned FAKE studies for various target configurations and neon-hydrogen mixtures as well as for plate arrangements. The results obtained on the basis of kinematical data from reference (7) are displayed in fig. 13. Whereas track sensitive targets surrounded by mixtures containing up to 100 °/o neon yield missing mass resolutions well below the neutral pion rest mass, the resolutions obtained under the assumption of plate arrays in BEBC are not sufficient to clearly discriminate against the neutral pion rest mass. The missing mass resolutions obtained for the heavy liquid chamber "Gargamelle"[20] are rather close to the neutral pion rest mass.

These FAKE studies indicate a 15 °/o fraction of the total energy which goes into the two neutral pions associated with the four prong. By setting in relation (15) Y = 0.15 and X = 5, which corresponds to the error ratio of neutral and charged pions obtained in case of a track sensitive target immersed in a 50 molar °/o mixture, we expect from relation (15) a 60 °/o increase of the missing mass. With conversion plates the error ratio becomes 25 and according to relation (15) this yields a missing mass which is 4.5 times that obtained for the charged secondaries. This is in fair agreement with the results obtained for there cases with the corresponding FAKE studies.

VIII. Conclusions

Extrapolation from present knowledge in elementary particle reactions to higher energy transfers establishes the certainty that neutral pion spectroscopy is inevitable for future event fittings (figs 1 and 2). From neutral pion decay we learned that sufficient gamma conversion and efficient gamma association are the fundamental requirements to achieve this goal. Sufficient gamma conversion dictates a minimum material layer which corresponds to about 2 radiation lengths (relations (5) (5a)). Efficient gamma association calls for high spatial resolution of the conversion points (relation (3a)) to provide precise angular measurements and for small gamma momentum errors (relation (3)) which in turn presupposes restrictions on the density of the conversion materials (relation (9)). Balancing the two opposing requirements for gamma conversion and gamma association requires sufficient detector volume to be available for neutral pion spectroscopy (relation (9a)).

High spatial resolution, e.g. better than 500 μm in real space, is a typical merit of bubble chamber liquids. Comparable resolutions can hardly be achieved with conversion plates if at the same time at least 2 radiation lengths for gamma conversion within a given detector volume are required. This is true for plate arrays in hydrogen/deuterium chambers, which pressupose curvature measurements of conversion pairs between two subsequent plates, as well as for conversion plates arranged in an electronic counter device like OMEGA [21]. In this case the radiation length of the plate material can be attenuated to that of a conversion liquid by providing a corresponding number of plates and spacings. This results in a negligible contribution of the plate error (relation 11) and curvature measurements of conversion pairs are then no longer restricted to the gap between two subsequent plates. Consequently, the relations for optimum track length (8) and minimum gamma momentum error (9a) which were derived for a track sensitive conversion liquid are also valid for such a plate distribution. By asking for equal gamma momentum errors under identical conditions for gamma

conversion efficiency and gamma momentum the total depth D_p' of such a plate distribution scales like:

$$D_p' = D_L \left(\frac{B_L \varepsilon_p}{B_p \varepsilon_L} \right)^{1/2}$$

with the symbold for plates and liquid labeled P and L, resp. With the foreseen magnetic flux density of BEBC being twice that of OMEGA the total depth for π^o- detection required in the counter device is 1.4 times larger. In this case we presuppose the same spatial resolution, for BEBC and for OMEGA, a condition hardly achievable with electronic counters arranged within the spacings of the conversion plates.

Provision of the required gamma conversion layer while maintaining at the same time a satisfactory gamma momentum resolution asks for matching the conversion liquid density to the geometrical dimensions of the bubble chamber. This is possible within an order of magnitude with neon-hydrogen fillings which exhibit thermodynamic parameters compatible with those of hydrogen or deuterium for chamber operation. Track sensitive hydrogen or deuterium targets can therefore be surrounded by neon-hydrogen conversion liquids. In this way the resulting composite chamber draws advantages from the merits of hydrogen/deuterium and heavy liquid chambers. With respect to elementary particle spectroscopy such devices are, at the time being, clearly superior to other competitors: With respect to gamma resolution they are preferable to conversion plates in hydrogen/deuterium chambers and they should, according to figs 8 and 10 achieve better missing mass resolutions than the hydrogen chambers of the 2 m - type. Finally, it is obvious from figs 9 and 13 that composite BEBC, equipped with fillings and targets as indicated, provides at least the same neutral pion detection efficiency but better missing mass resolutions than the heavy liquid chamber "Gargamelle"[20].

Flat target bags with flexible walls for pressure transmission cover mixture ranges up to 70 molar °/o neon fraction (45 cm radiation length) or probably up to 85 molar °/o Ne (33 cm radiation length) if we allow for 1°K temperature difference between hydrogen and mixture, and provide three geometrical dimensions to best fulfil the demands of neutral pion spectroscopy and missing mass resolution. The rigid target cylinders with attached bellows for pressure transmission allow for pressure differences between target liquid and conversion mixture, which could therefore consist in almost pure neon (28 cm radiation length), but are restricted with respect to shape optimisation. The FAKE results displayed in fig. 14, which shows the resolution efficiency for two neutral pions, clearly favour the flat target bags. Obviously, the more dense conversion liquid surrounding the cylindrical targets is overcompensated by the longer gamma conversion paths and the higher pairing efficiency offered by the flat bags and the lighter conversion mixtures associated with them. Since, according to fig. 13, the total missing mass resolution of both systems is almost the same, we prefer the technique which promises the higher fraction of event fits in BEBC.

Our FAKE results suggest for use with BEBC the following target dimensions: 300 cm in beam direction, about 100 cm for beam spread, and between 10 cm and 15 cm in the magnetic field direction. To summarize our principal concerns, which are event fit efficiency for deep inelastic collisions under typical PS conditions - charged multiplicity: four, and π^o- multiplicity: two - we obtain for BEBC the FAKE figures indicated in table 1. From this table we learn, that track sensitive hydrogen targets surrounded with neon-hydrogen mixtures at 16 GeV/c beam momentum already considerably increase the event fit efficiency obtained with a hydrogen filling in BEBC. According to figures 1 and 2 this behaviour is strongly amplified at higher beam momenta (Serpukhov, Batavia, CERN II).

Finally, we would like briefly to mention some other advantages of neon-hydrogen mixtures, which do not directly concern neutral pion spectroscopy, but which, in a more general consideration of particle detection, merit our attention. The momentum region where particle masses can be determined via the more precise range measurements rather than by their curvatures is largely extended due to the higher stopping power of the mixture. The same holds for particle discrimination, at the time being mostly performed by the time consuming and troublesome procedure of bubble counting, which is feasible in a simpler and more unambiguous way by range measurements or helix fits. This is particularly true for large chambers with high magnetic flux densities.

TABLE 1 : Event fit efficiency of the 16 GeV ($\pi^- p$) - four prong channel obtained by FAKE studies with various BEBC configurations. The input rates correspond to the cross-sections reported in reference (7). They refer to inelastic events only whereas the no-fits in fig. 1 are normalized to the total cross-section (including elastic events). The two and six prongs show almost the same event fractions.

BEBC CONFIGURATION	EVENT TYPE	NORMALIZED EVENT RATES			
		INPUT	4C FIT	1C FIT	TOTAL FITS
Hydrogen Filling	4 prong	15	14.0		14.0
	4 prong 1 π^o	16	0.4	14.8	15.2
	4 prong 2 π^o	69	0.06	1.7	1.8
	total	100	14.5	16.5	31.0
Cylindrical Target Pure neon	4 prong	15	13.8		13.8
	4 prong 1 π^o	16	10.4	5.2	15.6
	4 prong 2 π^o	69	24.9	28.6	53.5
	total	100	49.1	33.8	82.9
Flat Target 70 mole % Neon	4 prong	15	13.5		13.5
	4 prong 1 π^o	16	11.6	4.1	15.7
	4 prong 2 π^o	69	37.8	22.2	60.0
	total	100	62.9	26.3	89.2
Flat Target 50 mole % Neon	4 prong	15	13.5		13.5
	4 prong 1 π^o	16	10.0	5.6	15.6
	4 prong 2 π^o	69	27.3	26.7	54.0
	total	100	50.8	32.3	83.1
Flat Target 40 mole % Neon	4 prong	15	13.5		13.5
	4 prong 1 π^o	16	8.6	6.9	15.5
	4 prong 2 π^o	69	21.3	28.6	49.9
	total	100	43.4	35.5	78.9
Flat Target 30 mole % Neon	4 prong	15	13.5		13.5
	4 prong π^o	16	6.8	8.5	15.3
	4 prong π^o	69	13.4	31.7	45.1
	total	100	33.7	40.2	73.9

References

(1) E. Pickup, D.K. Robinson, E.O. Salant, F. Ayer and B.A. Munir: Phys. Rev. 132 (1963), 1819

(2) P. Daronian et al.: Nuovo Cimento 41 (1966), 503

(3) Saclay-Orsay-Bari-Bologna collaboration: Nuovo Cimento 29 (1963), 515

(4) F.E. James et al.: Phys. Rev. 142 (1966), 896

(5) Aachen-Birmingham-Bonn-Hamburg-London-München collaboration: Nuovo Cimento 31 (1964), 485 and 729

(6) Aachen-Berlin-CERN collaboration: Nuclear Physics B 8 (1968), 45

(7) Aachen-Berlin-Bonn-CERN-Cracow-Heidelberg-Warsaw collaboration: Nuclear Physics B 13 (1969), 571

(8) J.W. Elbert, A.R Erwin, W.D. Walker and J.W. Waters: Nuclear Physics B 19 (1970), 85

(9) O. Czyzewski and K. Rybicki: Inst. Nucl. Phys. Report 703/PH Krakow 1970

(10) G.H. Trilling: SLAC report 5-E (1962)

(11) D. Morellet: HERCEG NOVI (1968)

(12) H. Leutz and G. Rau: CERN/TC/BEBC 65-3 and CERN/TC/BEBC 66-73

(13) C.M. Fisher: CERN/TCC 71-12 (1971)

(14) D.J. Miller: CERN/TCC 71-13 (1971)

(15) H. Leutz: Proceedings of the International Conference on Bubble Chamber Technology, Argonne (1970)

(16) H. Leutz: CERN/TC/BEBC 66-21 (1966)

(17) Z. Strugalski: JINR report R 796/61 (1961)

(18) H. Burmeister, G. von Dardel and K. Schultze: CERN/NPA 63-22 (1963)

(19) R. Arnold, I.A. Budagov, F. Nezrick and W. Venus: CERN/NPA 68-9 (1968)

(20) Gargamelle Construction Group: The large heavy liquid chamber "Gargamelle", Proc. Intern. Colloq. Bubble chambers, CERN 67-26 (1967)

(21) The Omega Project: CERN/NP/68-11 (1968)

(22) H. Wenninger: CERN/TCC/71-15 (1971)

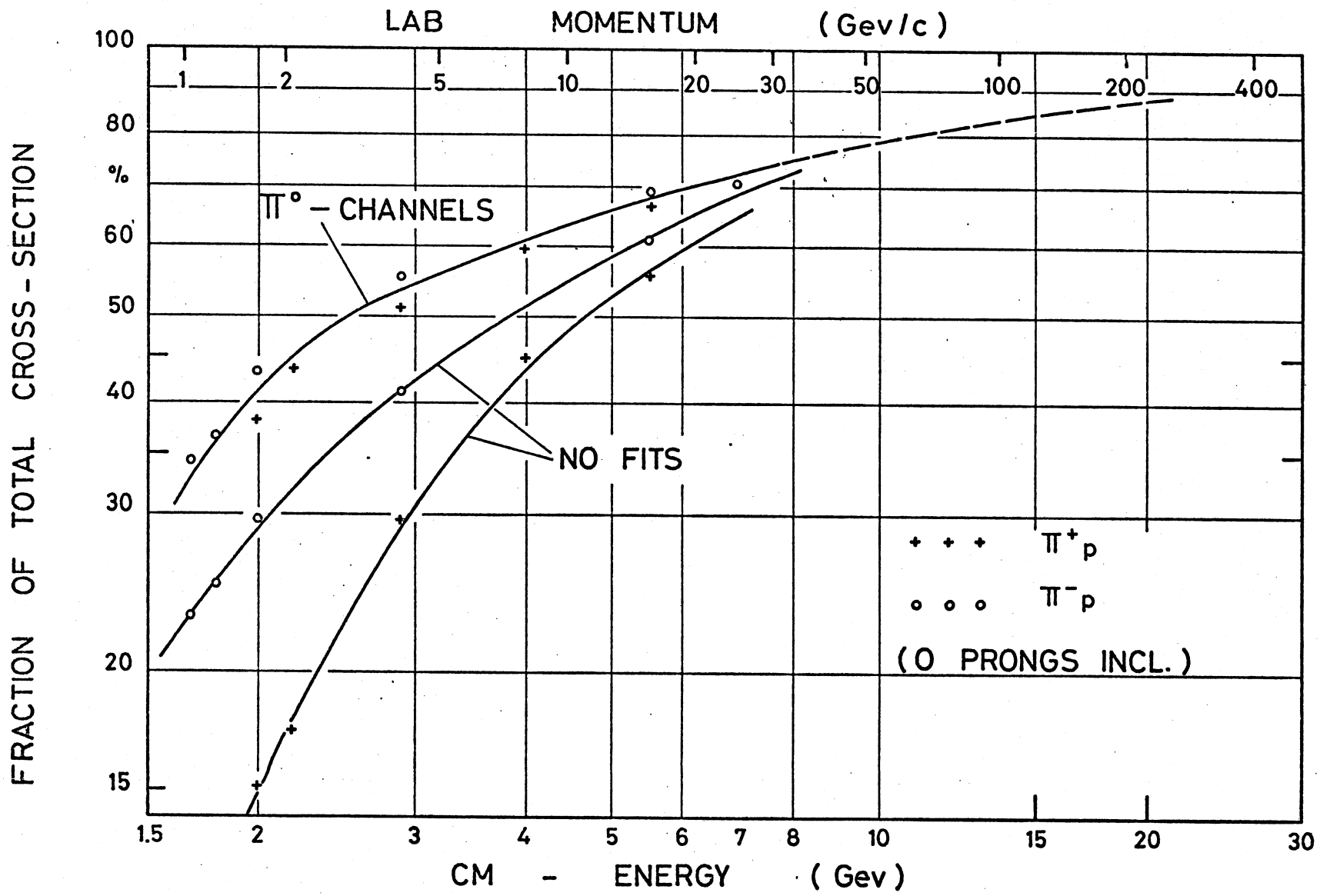

Fig. 1 Fractions of ($\pi^{\pm}$ p) total cross-sections going into π^{o}- channels and unfitting events. The data were extracted from references (1) - (8).

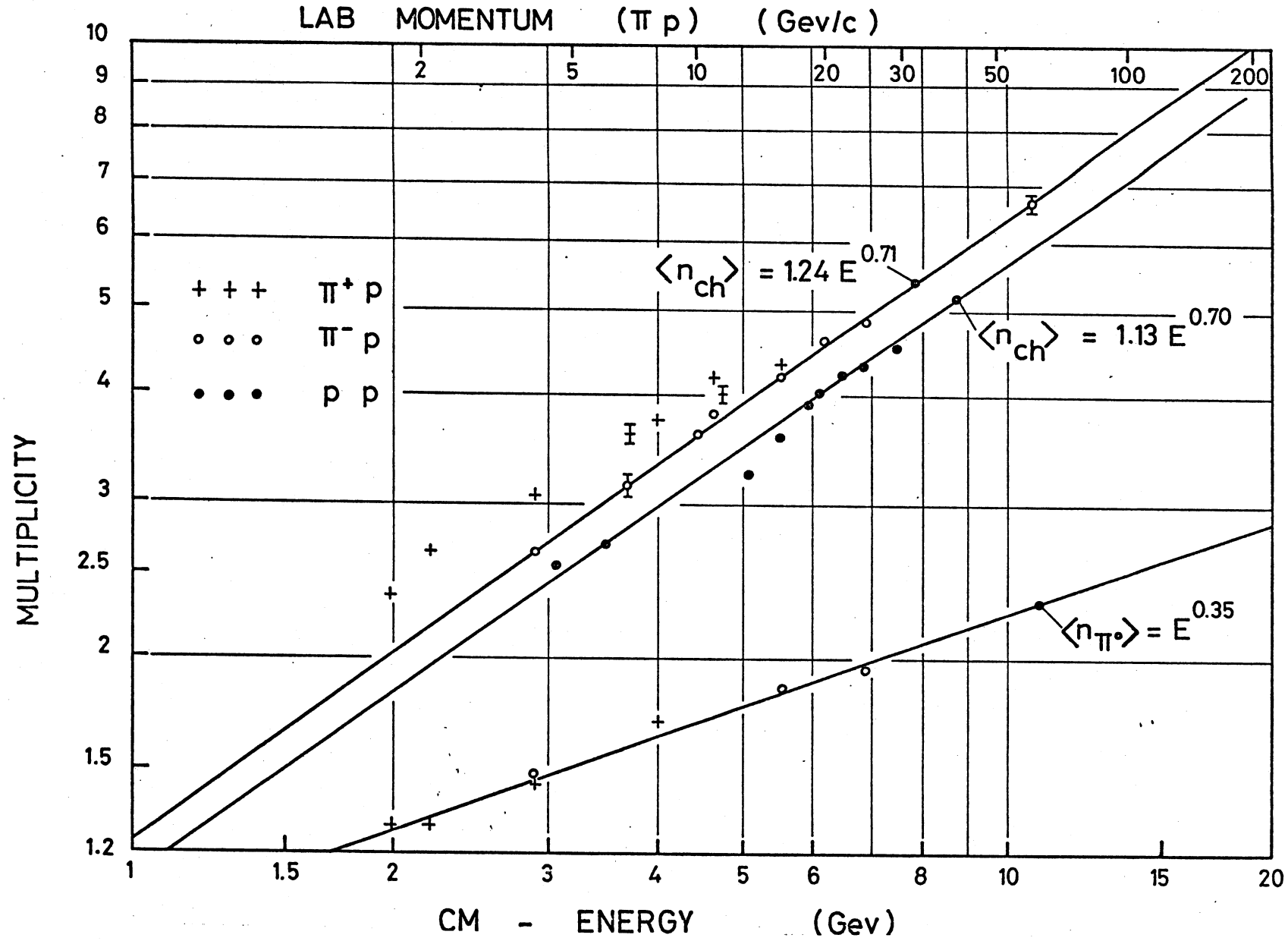

Fig. 2 Multiplicities of charged particles computed by O. Czyzewsky and K. Rybicki [9] and of neutral pions calculated from cross-sections quoted in references (1) - (8)

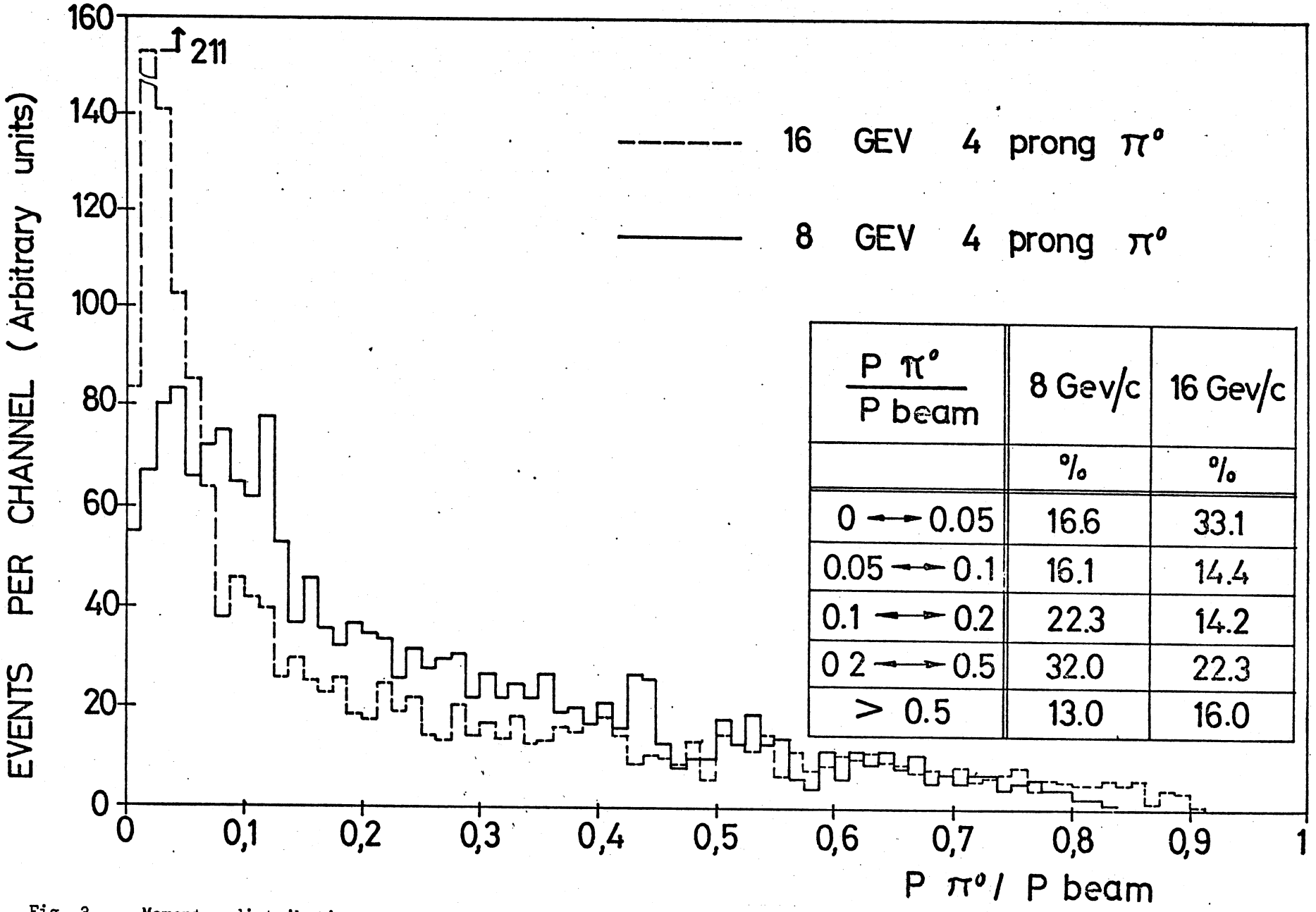

P π° / P beam	8 Gev/c	16 Gev/c
	%	%
0 ⟷ 0.05	16.6	33.1
0.05 ⟷ 0.1	16.1	14.4
0.1 ⟷ 0.2	22.3	14.2
0 2 ⟷ 0.5	32.0	22.3
> 0.5	13.0	16.0

Fig. 3 Momentum distribution, normalized to the beam momentum, of single produced neutral pions. The data were extracted from references (6) and (7).

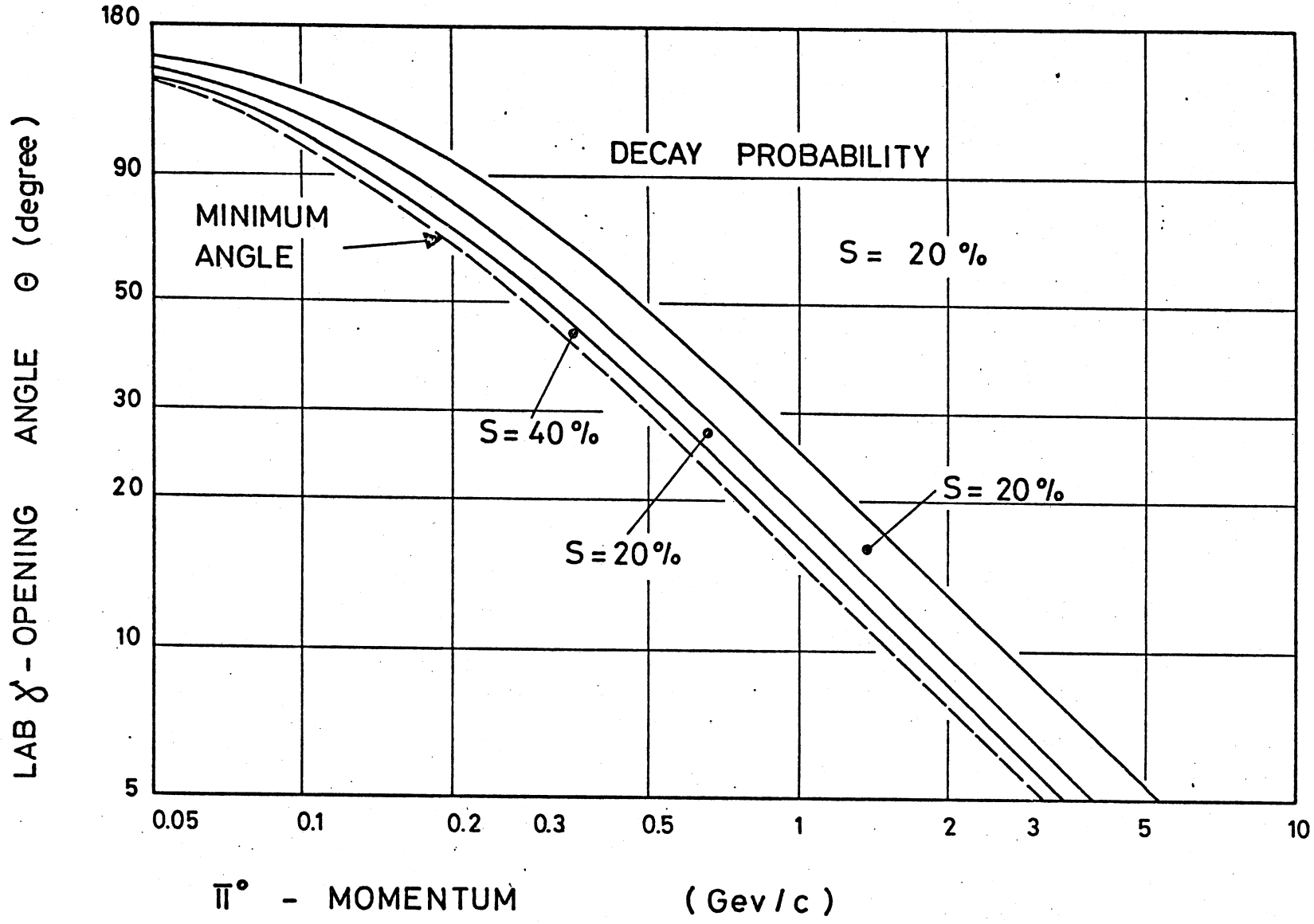

Fig. 4 Probability distributions for the gamma opening angles in the lab system.

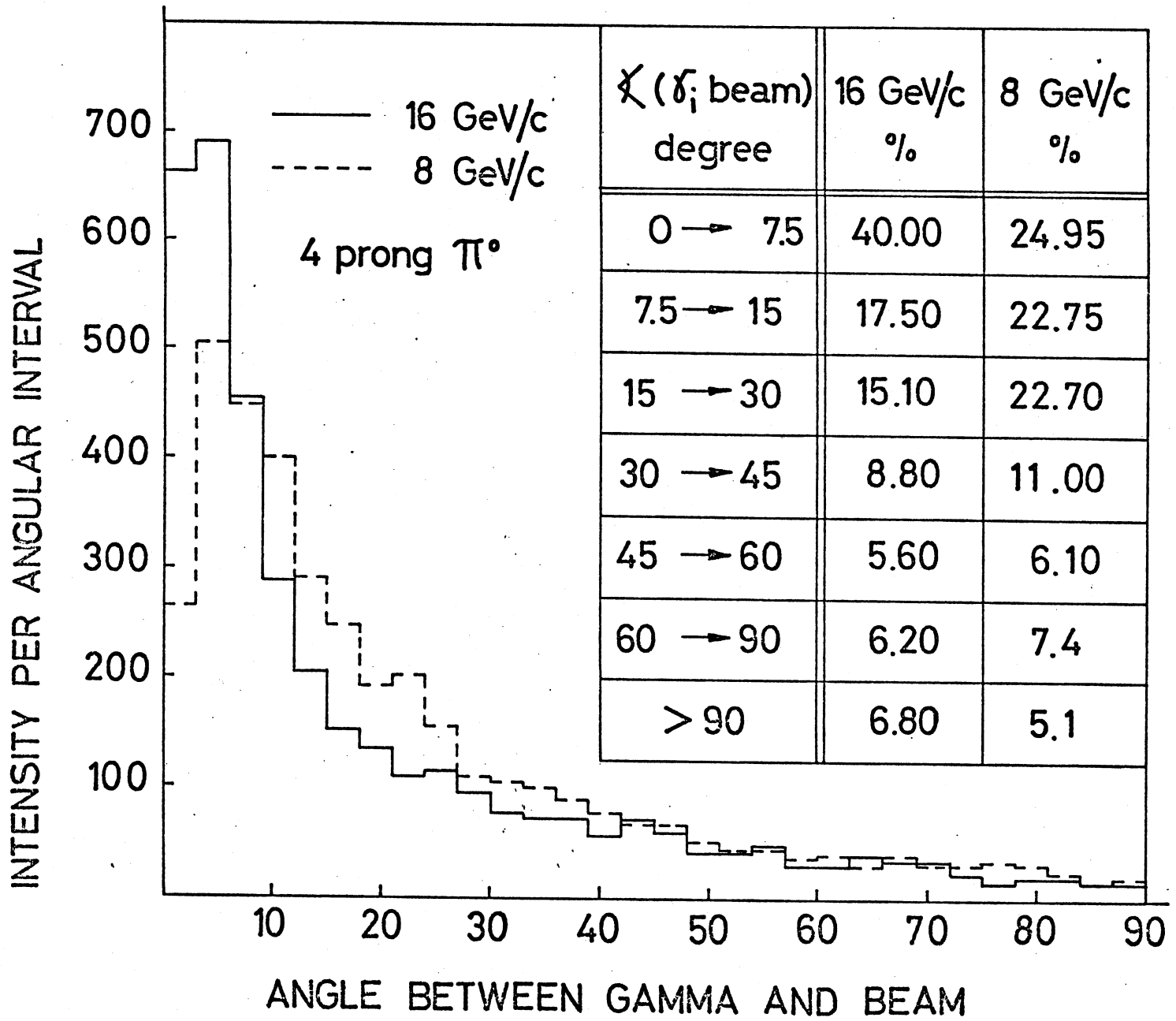

∠(γ_i beam) degree	16 GeV/c %	8 GeV/c %
0 → 7.5	40.00	24.95
7.5 → 15	17.50	22.75
15 → 30	15.10	22.70
30 → 45	8.80	11.00
45 → 60	5.60	6.10
60 → 90	6.20	7.4
> 90	6.80	5.1

Fig. 5 Gamma angular distributions from single produced neutral pions. The data were extracted from references (6) and (7)

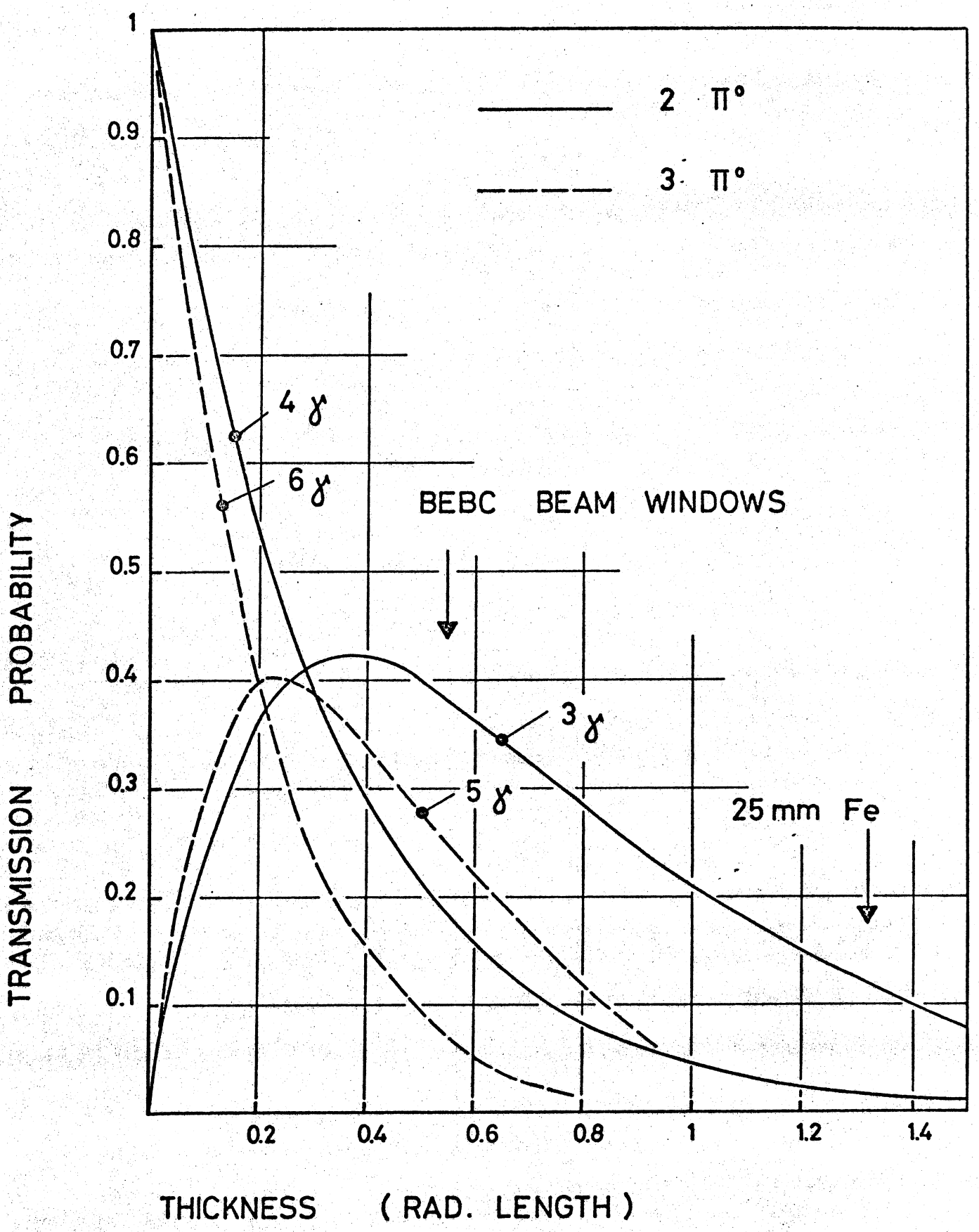

Fig. 6 Transmission probabilities for six and five gammas emerging from three neutral pions, and for four and three gammas emerging from two neutral pions.

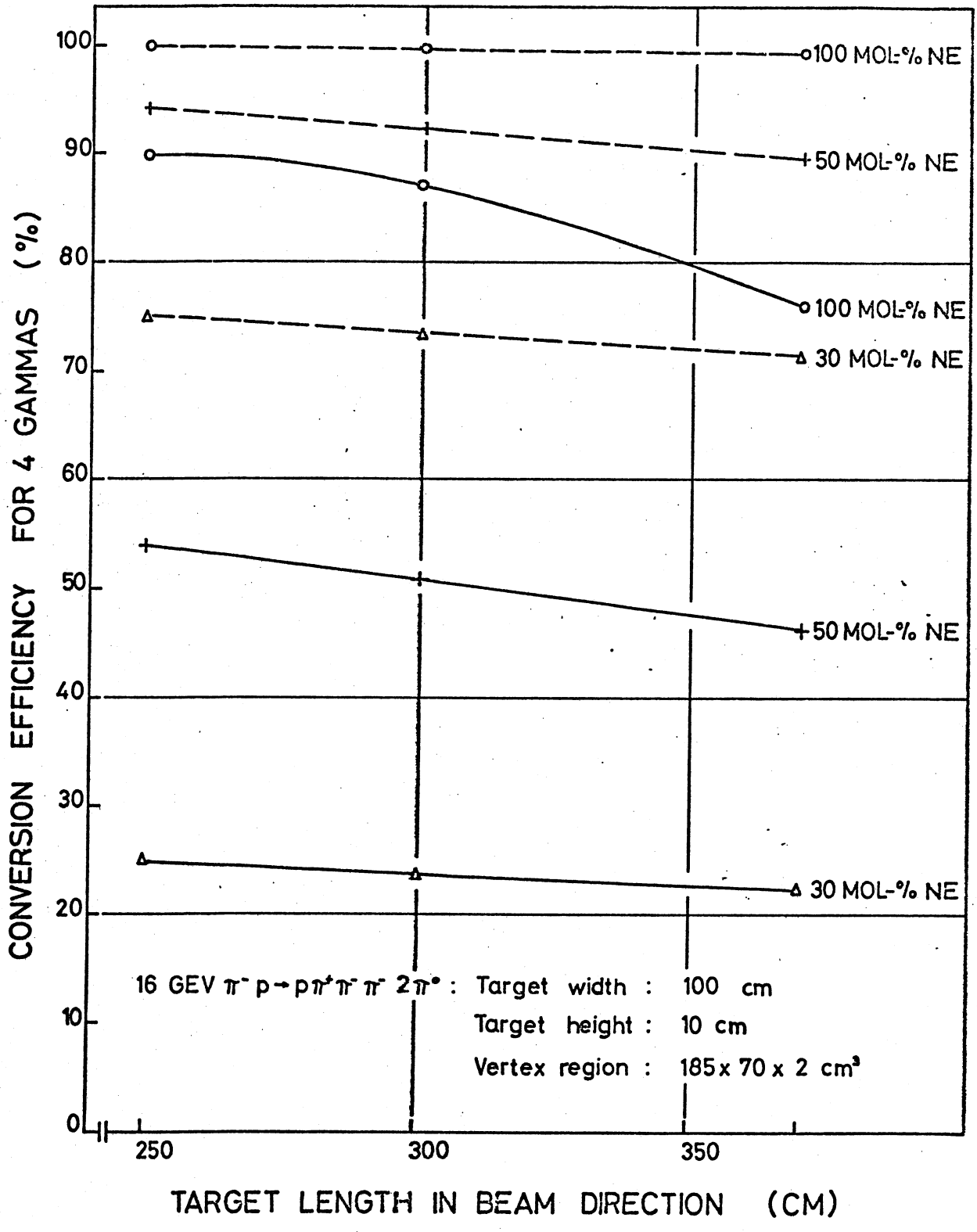

Fig. 7 Conversion efficiencies for four gammas (solid curves) and for three gammas (dashed curves) from two neutral pions. The data were obtained by FAKE simulations based on the DST of reference (7) and on the BEBC fiducial volume.

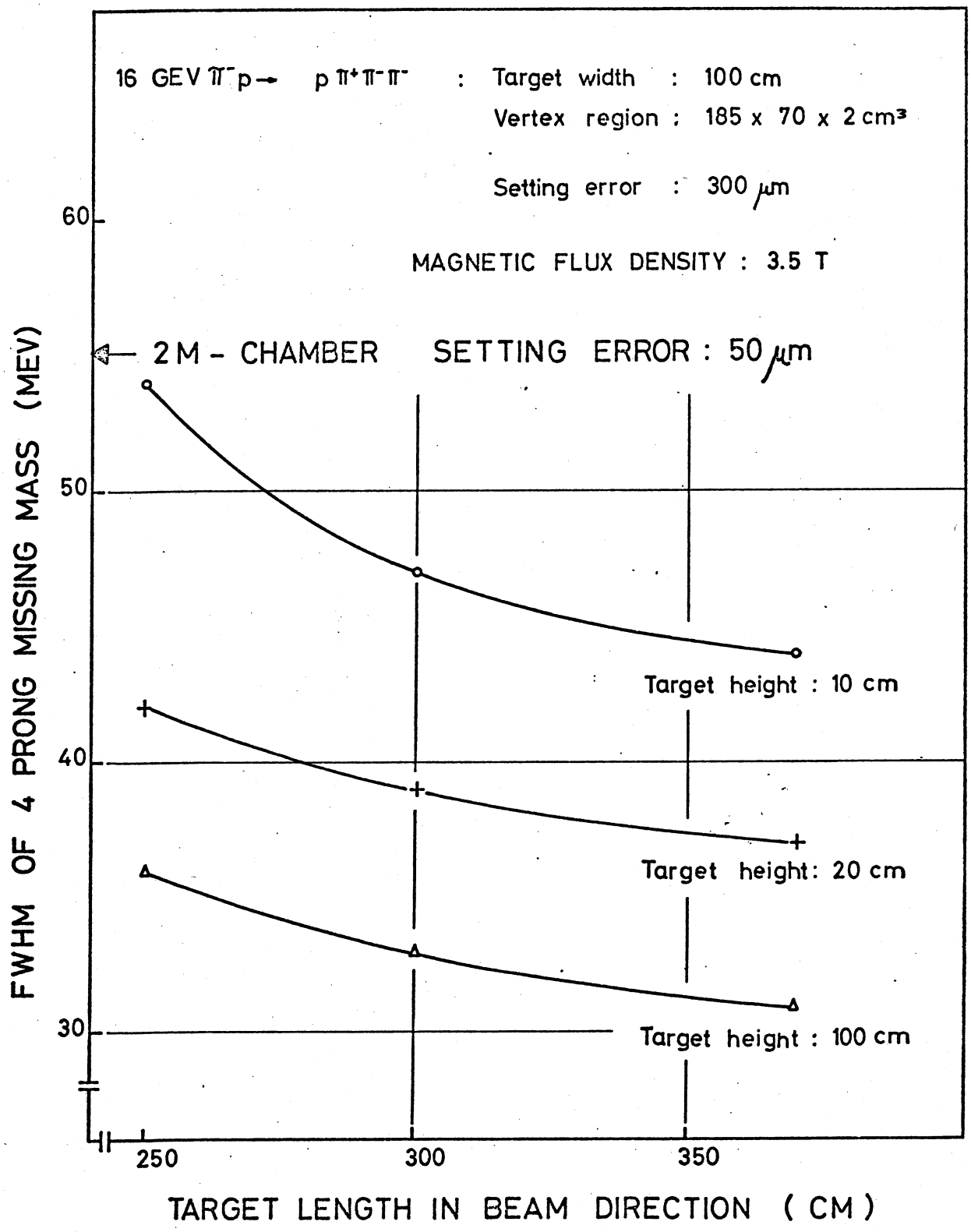

Fig. 8 Missing mass resolutions of four prong events faked under BEBC conditions from kinematical data which have been extracted from the DST of reference (7). The 300 μm setting error assumed for BEBC should be achievable provided the optical chamber constants are reasonably well determined.

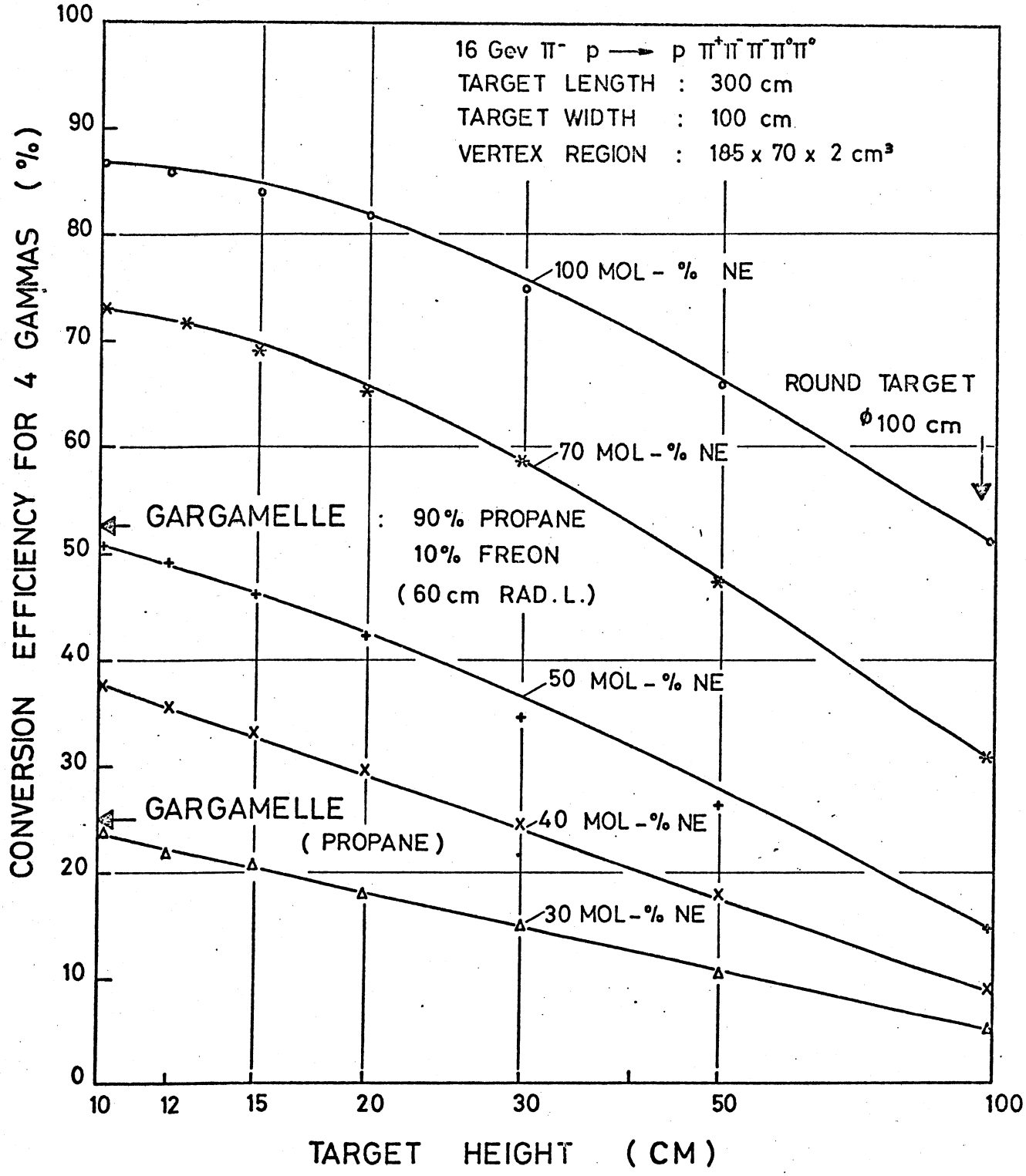

Fig. 9 Conversion efficiencies for four gammas from two neutral pions. The curves refer to flat target bags in BEBC and the values at 95 cm target height correspond to the conversion efficiencies obtained with cylindrical targets of 300 cm length in BEBC. Again, the FAKE simulations were based on the DST of reference (7).

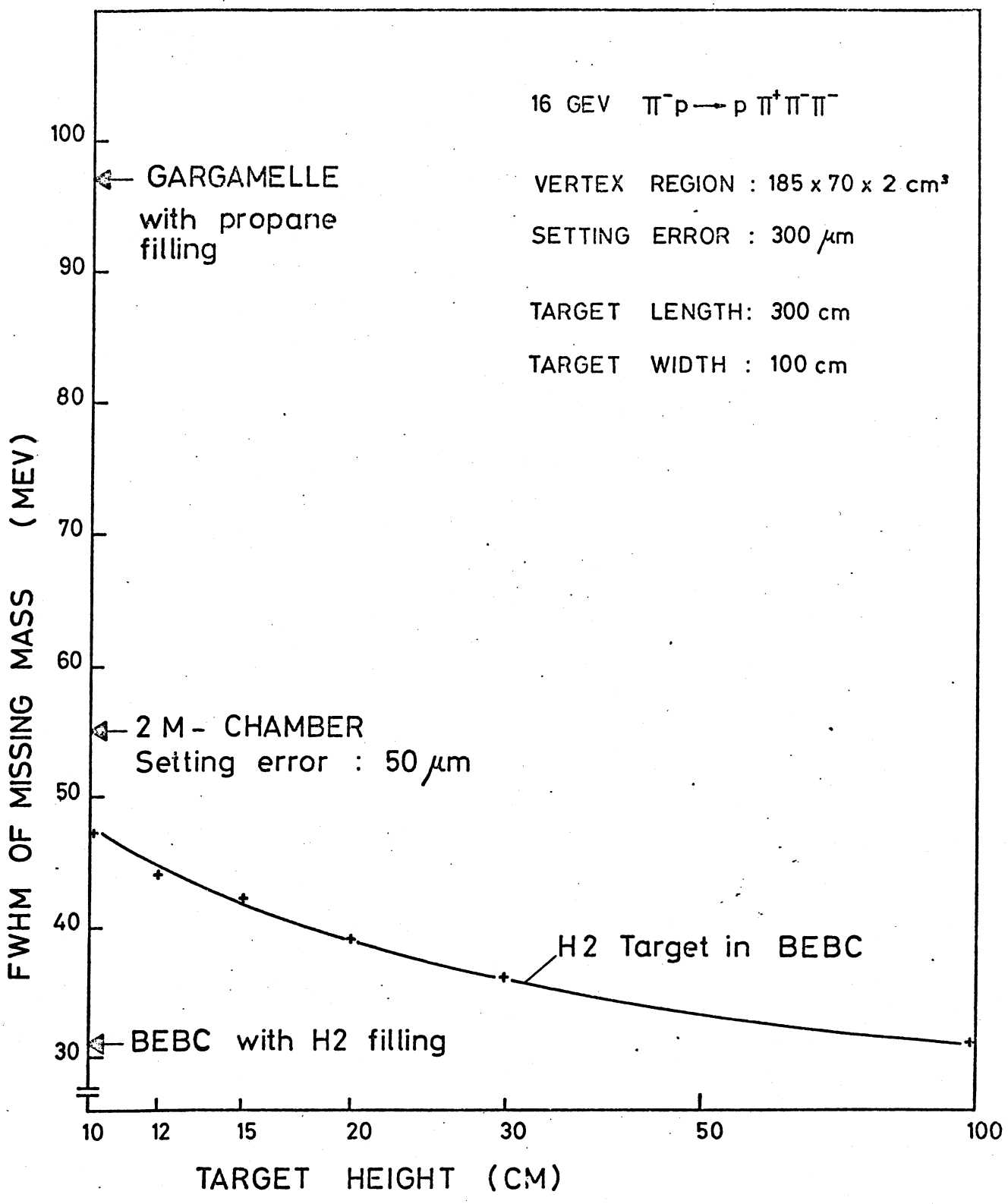

Fig. 10 Missing mass resolution of four prong events faked under BEBC and Gargamelle conditions. The kinematical data and the resolution indicated for the 2m chamber were taken from the DST of reference (7)

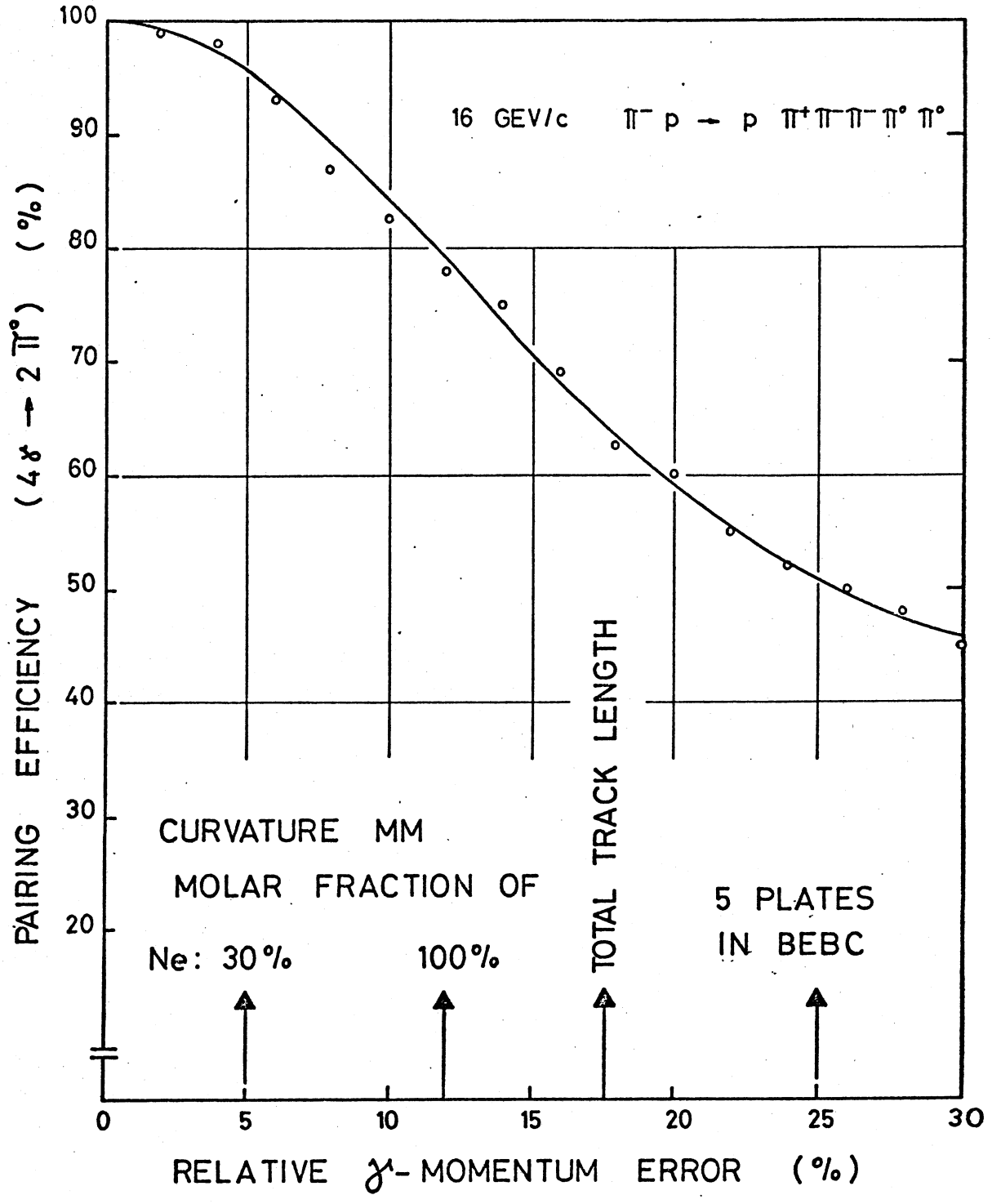

Fig. 11 Influence of gamma momentum error on the association of gamma pairs with the parent neutral pion. The gamma kinematical data were computed from the momenta of two opposite charged pions in the six prongs of reference (7) and were filtered through the χ^2- fit of relation (3). Ambiguities due to converted bremsstrahlung quanta were not taken into account. They would also depend on the radiation length of the conversion liquid and therefore the slope with the gamma error would be amplified.

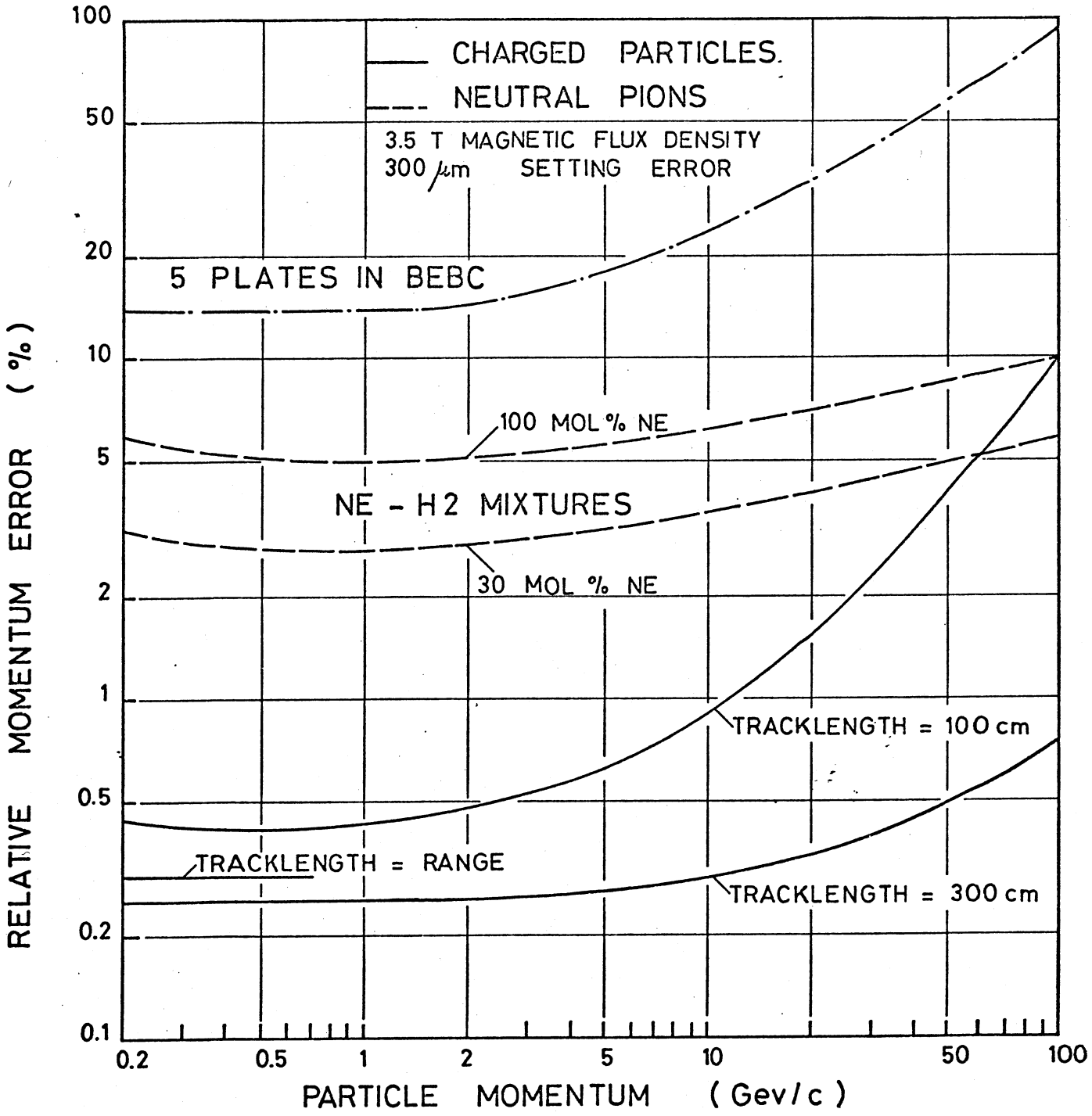

Fig. 12 Relative momentum errors for charged particles and for neutral pions calculated with the assumption of curvature measurements in BEBC. The momentum region indicated for range measurements of charged secondaries was obtained from FAKE studies based on the 16 GeV/c (Π^-p) - experiment [7].

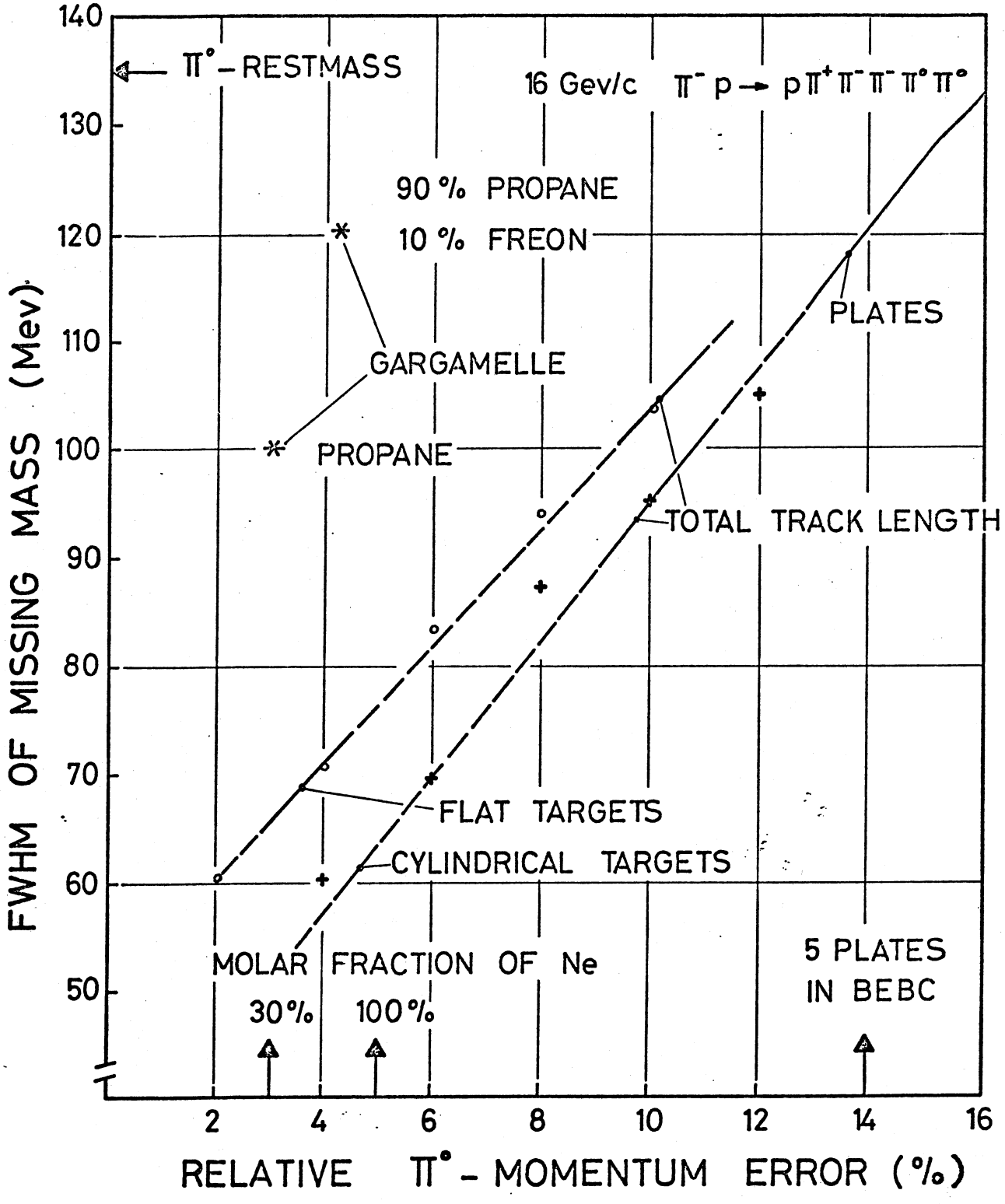

Fig. 13 Missing mass resolutions of 4 prongs with two neutral pions. Track sensitive targets and plates were considered as being mounted in BEBC. Again, the FAKE studies were based on the kinematical data from reference (7).

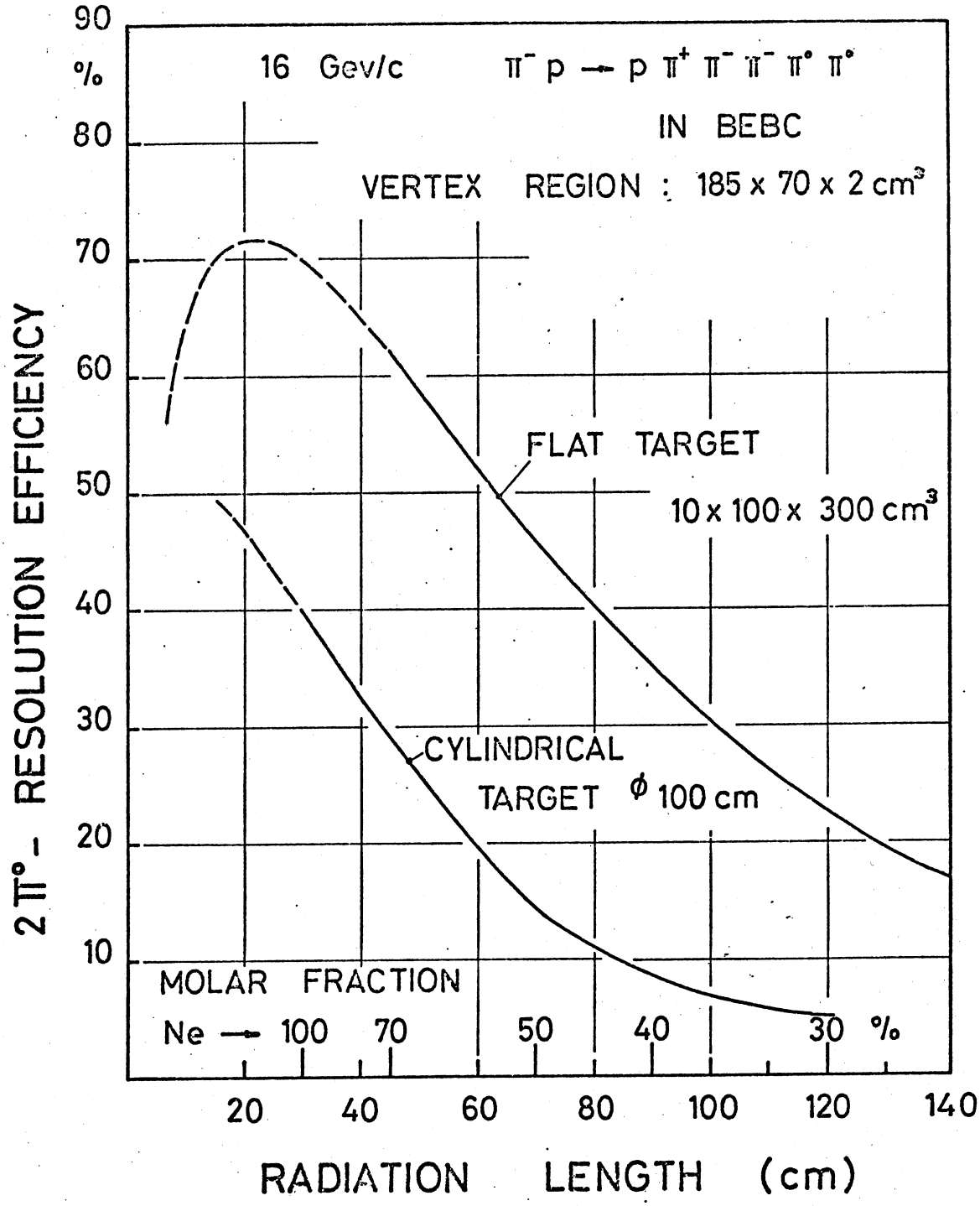

Fig. 14 The product of conversion efficiency (fig. 9) with the pairing efficiency (fig. 11) yields the resolution efficiency for production channels containing two neutral pions.